Article (refereed) - postprint

Oliver, Rebecca J.; Taylor, Gail; Finch, Jon W.. 2012 Assessing the impact of internal conductance to CO2 in a land-surface scheme: measurement and modelling of photosynthesis in Populus nigra. *Agricultural and Forest Meteorology*, 152. 240-251. 10.1016/j.agrformet.2011.10.001

Assessing the impact of internal conductance to CO_2 in a land-surface scheme: Measurement and modelling of photosynthesis in *Populus nigra*

Rebecca. J. Oliver [a,b], Gail Taylor [b] and Jon. W. Finch [a]

[a] Centre for Ecology and Hydrology, Benson Lane, Wallingford, Oxfordshire, OX10 8BB, UK

[b] School of Biological Sciences, University of Southampton, Highfield Campus, Southampton, SO17 1BJ, UK

Abbreviations:

Atmospheric CO_2 concentration (c_a); intercellular CO_2 concentration (c_i); chloroplastic CO_2 concentration (c_c); net photosynthesis (A_{net}); stomatal conductance (g_s); maximum carboxylation rate of Rubisco (V_{max}); maximum rate of electron transport (J_{max}); internal CO_2 conductance (g_i); intrinsic quantum efficiency (α_{int}); apparent quantum efficiency (α_{app}); c_i/c_a ratio for specific humidity deficit in the canopy (F_0); critical humidity deficit (D_c)

Abstract

Vegetation plays a key role in both the global carbon and water cycles. Therefore, the representation of leaf-level fluxes of carbon and water in process-based land-surface schemes is central to accurately predicting these surface exchanges on a larger scale. Leaf-level models of photosynthesis used in such schemes are commonly based on the equations of Farquhar *et al*., (1980), which were founded on the assumption that differences in the drawdown of CO_2 from sub-stomatal cavities (c_i) to the site of carboxylation inside chloroplasts (c_c) were negligible. Recent research, however, indicates an important role for this additional internal pathway of CO_2 transfer (g_i) in photosynthesis. This work therefore combined fieldwork and modelling to assess the impact of g_i on estimation of key photosynthetic parameters, and on the accuracy of simulated photosynthesis (A_{net}) and stomatal conductance (g_s) in a coupled model of leaf-level A_{net} and g_s embedded in a land-surface scheme. It was shown that, in a fast growing poplar genotype (*Populus nigra*), the photosynthetic parameter V_{max} was sensitive to g_i. Determination of V_{max} under the assumption of finite g_i led to estimates of V_{max} in well-watered trees that were, on average, 52 % higher than values calculated on a c_i basis. Drought induced declines in all key photosynthetic parameters measured were observed (V_{max}, J_{max}

and g_i), in addition to a two-fold increase in photosynthetic biochemical capacity upon re-watering. Reasons for this and the implications for land-surface modelling are discussed. It was shown that inclusion of a constant (non-water stressed) internal conductance to CO_2 in a coupled model of leaf-level A_{net} and g_s did not improve the accuracy of these simulated fluxes. It was concluded that, for application within a land-surface scheme, currently, accurate calibration of V_{max} potentially has a greater impact on simulated A_{net} and g_s than the inclusion of additional, fine-scale leaf-level processes such as g_i.

Keywords: land-surface model, poplar, gas exchange, V_{max}, mesophyll conductance

1. Introduction

From the gains and losses of carbon through photosynthesis and respiration, and the passage of water through plant stomata to the atmosphere, vegetation plays a major role in both the global carbon and water cycles. For land-surface schemes to correctly simulate carbon and water budgets, they must accurately represent the processes of carbon and water exchange from vegetated surfaces. Land-surface schemes commonly model carbon exchange of vegetation using biochemical models of leaf-level photosynthesis based on the equations of Farquhar *et al*., (1980), coupled to a stomatal conductance model to simulate leaf-level fluxes of carbon dioxide and water. These are then scaled up to simulate carbon and water exchanges at the canopy-level. Therefore, correct parameterisation of these models at the leaf-level is central to accurate predictions of vegetation productivity and water-use at the larger-scale. The work of Hughes *et al*., and Vanloocke *et al*., (2010) for example, both used land-surface schemes to determine the carbon- and water-balances respectively of extensive plantings of *Miscanthus x giganteus*, a C_4 perennial grass bioenergy crop. Used in applications such as these, it is imperative that models are parameterised appropriately, and that simplifications used to represent key processes in models are adequate.

Until recently, photosynthesis in plants was considered to be limited dominantly by two factors; g_s, which regulates the CO_2 supply into the leaf, and leaf biochemistry, which is the basic photochemistry, carboxylation and Calvin cycle reactions that regulate the CO_2 demand (Flexas et al., 2008). Consequently, models of photosynthesis, such as Farquhar *et al*., (1980) and Collatz *et al*., (1991; 1992), were founded on the assumption that differences in the CO_2 concentration in the sub-stomatal cavities and at the site of carboxylation in the chloroplast stroma were negligible. In other words, c_i (the intercellular CO_2 concentration) was equal to c_c (the chloroplastic CO_2 concentration). Recent research, however, identified the important role of internal CO_2 conductance (g_i) in regulating

68 photosynthesis, i.e. the transfer of CO_2 across mesophyll cells from c_i to c_c. There is increasing
69 evidence suggesting that g_i is actually finite and can itself respond to changing environmental
70 conditions, such that it can impose a significant limitation on photosynthesis (Centritto et al., 2003;
71 During, 2003; Flexas et al., 2007a; Flexas et al., 2002; Grassi and Magnani, 2005; Warren et al.,
72 2004). Current research suggests that g_i is of similar quantitative importance to stomata and Rubisco
73 in terms of limiting/regulating photosynthesis (Ethier and Livingston, 2004; Flexas et al., 2008;
74 Warren, 2008). Therefore, it is suggested that it may be necessary to re-formulate photosynthesis
75 models to include this process in order to improve predictions of leaf-level carbon assimilation
76 (Ethier and Livingston, 2004; Flexas et al., 2008; Niinemets et al., 2009).
77
78 The present study addresses two questions: (1) what is the impact of internal conductance to CO_2 (g_i)
79 on estimates of the key photosynthetic parameters V_{max} (the maximum rate of carboxylation at
80 Rubisco) and J_{max} (the maximum rate of electron transport) in *Populus nigra*? (2) does the inclusion
81 of this additional pathway of CO_2 transfer in a coupled model of leaf-level photosynthesis – stomatal
82 conductance improve the accuracy of these two simulated fluxes? CO_2- and light-response curves
83 were measured on a variety of poplar (*P. nigra* L.) to determine the impact of g_i on estimates of the
84 key photosynthetic kinetic parameters. This data was used to test and calibrate a coupled model of
85 leaf-level photosynthesis and stomatal conductance embedded in a land-surface scheme called
86 JULES (Best et al., 2011; Clark et al., 2011). The leaf-level model was modified to include the
87 transfer of c_i to c_c to assess the impact of g_i on the accuracy of predicted photosynthesis and stomatal
88 conductance. An independent data set was used to validate the performance of the different model
89 configurations.
90
91 **2. Materials and Methods**
92
93 **2.1. Plant material and experimental setup**
94
95 Established cuttings of *P. nigra* L. (cv. Jean Pourtet) were cultivated at Wytham field station
96 (Wytham, Oxfordshire, UK; 51°44'99"N, 1°18'97"W). In April 2008, the cuttings were potted into
97 10 L pots (300 mm diametre x 250 mm depth) using a soil-based, lime-free compost (John Innes No.
98 3). Fifty trees (25 per treatment) were arranged in a split-plot design. Trees were randomly
99 distributed between four blocks. Two blocks were subject to periods when water was withheld to
100 impose a drought treatment. The remaining two blocks were watered continuously over the course of
101 the experiment. A_{net} and g_s were measured over the course of the experiment under ambient
102 atmospheric conditions. Recordings were made from at least four, and up to ten trees per block, per
103 treatment at each measurement period (before, during and after each drought period). Trees were

chosen at random, and measurements were made on the first fully expanded, sun-exposed leaf (i.e. one leaf per tree). Three recordings on the same leaf were made, and the average of these was used in analyses. Measurement of response curves used three trees per treatment, and the same trees were used over the course of the experiment. Trees had been selected at random from the blocks, and curves were measured on the first fully expanded leaf of each tree.

Before the onset of experiments all trees were fully watered. Pots were spaced at 300 mm intervals to avoid shading and allow access to the trees. Watering treatments began when leaves were completely developed and matured. Control trees were continuously watered so their soil moisture content remained near to field capacity (around 30 % volume). For the duration of the experimental period, mean soil moisture of control trees was 30.6 % vol. ± 3.5 %vol. Stressed trees endured two periods of imposed soil water stress where they were not watered and pots were shielded from rainfall by the use of a polythene cone fitted around the base of the stem and the lip of the pot so the canopy remained exposed to the atmosphere. The protective covers could be raised and lowered as necessary to allow circulation of air beneath during dry periods. Any effect of the use of these covers on soil temperature was deemed minimal when compared to the effect of reduced moisture content on soil temperature. In total, water was withheld for 25 days (2 to 26 June) during the first drought cycle; trees were then fully re-watered for eight weeks until the onset of the second drought cycle, which lasted 40 days (20 August to 28 September). In both drought cycles, plants were kept without water until net photosynthesis was almost completely inhibited during the late morning.

2.2. Soil moisture

Soil moisture content was monitored continuously over the course of the experiment using SM200 soil moisture sensors (Delta-T Devices Ltd, Cambridge, UK). Soil moisture was recorded as % volumetric water content (% vol.). Twelve sensors in total were used, so soil moisture content of six trees per treatment could be continuously logged. Point measurements were also made to check the soil moisture content of pots without sensors.

2.3. Leaf-gas exchange measurements

Leaf-level gas exchange was recorded using a portable infrared gas exchange analyser (IRGA) system (CIRAS-2, PP-systems, Hitchin, UK). For all measurements, the leaf area used was 250 mm^2. *P. nigra* is amphistomatous so the stomatal ratio was maintained at 30% for the upper- and 70% for

the lower-leaf surface. This ratio had been determined from previous measurements of the contribution of stomata on the abaxial and adaxial leaf surfaces to the rate of g_s in this genotype (Ingmar Tulva *pers. comm.*, 2007).

2.3. Leaf-gas exchange under ambient atmospheric conditions

Leaf-level A_{net} and g_s were measured *in situ* under ambient atmospheric conditions over the course of the experiment. Measurements were made during the hours 09:00-12:00 GMT, and were restricted to days with clear skies; temperature and relative humidity inside the leaf chamber were close to ambient values. The CO_2 concentration inside the leaf chamber was maintained at 380 ± 5ppm using a CO_2 cartridge plugged into the CIRAS-2.

2.4. CO_2 response curve

The response of A_{net} to increasing concentrations of c_i was measured *in situ* using the IRGA system. Measurements were made between the hours of 09:00 and 14:00 GMT. Leaf temperatures were set at 25 ºC for all measurements, leaves were illuminated using a red-blue LED light source attached to the gas exchange system and photosynthetic photon flux density (P_{PFD}) was maintained at 1500 µmol m^{-2} s^{-1}. According to Bernacchi *et al.*, (2003) this level of P_{PFD} is just above the light saturation point for this species. Leaf vapour pressure deficits were maintained close to ambient. Following protocols suggested by Long and Bernacchi (2003) and Bernacchi et al., (2003), leaves were incubated at a CO_2 concentration of 200 ppm for 20-30 minutes prior to measurement to maximise stomatal opening. Measurement of A_{net} - c_i curves followed the method of Bernacchi et al. (2003) starting at 400 ppm CO_2, decreasing stepwise to 50 ppm, then increasing stepwise to 1800 ppm CO_2.

The A_{net} - c_i curves were fitted using the method of Sharkey *et al.*, (2007) to provide optimised estimates of g_i (µmol m^{-2} s^{-1} Pa^{-1}), V_{max} (µmol CO_2 m^{-2} s^{-1}) and J_{max} (µmol electrons m^{-2} s^{-1}). An online analytical tool to aid with curve fitting can be found at: www.blackwellpublishing.com/plantsci/pcecalculation. This method uses the biochemically based model for photosynthesis of Farquhar *et al.*, (1980) with modifications for finite internal CO_2 transfer (g_i), which uses c_c instead of c_i where $c_c = c_i - A/g_i$. This model was then adapted to calculate V_{max} and J_{max} at c_i, where $c_c = c_i$. For more information see Sharkey *et al.*, (2007) and Pons *et al.*, (2009).

2.5. Light response curve

Leaves were sampled as described for A_{net} - c_i measurements above. Leaves were placed in the leaf chamber and illuminated until steady-state rates of A_{net} and g_s had been achieved. Leaf temperature was set at 25 ºC for all measurements and CO_2 concentration was maintained at 380 ppm. A_{net} - P_{PFD} response curves were then measured starting at saturating light (2000 μmol m^{-2} s^{-1}) and decreased stepwise to darkness.

The A_{net} - P_{PFD} response curves were analysed using the software 'Photosynthesis Assistant' (Parsons and Ogston, 1998), which uses the equation given by Prioul & Chartier (1977). The software fits the equation through an iterative process to give parameter values associated with the smallest error.

2.6. Models

2.6.1. The coupled model for leaf-level photosynthesis and stomatal conductance

The photosynthesis – stomatal conductance model used in this work is embedded in the land-surface scheme JULES (Best et al., 2011; Clark et al., 2011), hereafter referred to as the JULES A_{net} - g_s model. This sub-model calculates the leaf-level exchanges of carbon and water. These are described as being dependent on a number of environmental variables as well as c_i, with an additional direct dependence on soil moisture status. This sub-model is based on the photosynthesis model of Collatz *et al.*, (1991) for C_3 plants and Collatz *et al.*, (1992) for C_4 plants, and uses the stomatal closure described by Jacobs (1994).

2.6.2. Overview of the modelling

The measured A_{net} - c_i and A_{net} - P_{PFD} response curves provided parameter values for *P. nigra* to test and calibrate the JULES A_{net} - g_s model. The JULES A_{net} - g_s model was used in the following configurations;1) the original configuration 2) modified to include the transfer of CO_2 from c_i to c_c, and 3) modified to use the photosynthesis model of Farquhar *et al.*, (1980) and include internal CO_2 conductance. The accuracy of simulated A_{net} and g_s was compared in these three different model configurations. Model testing, calibration and validation occurred in three steps:

i) The performance of each model configuration was tested after being parameterised with individual values for the photosynthetic parameters taken from separate A_{net} - c_i and A_{net} - P_{PFD} response curves. The accuracy of simulated A_{net} in response to increasing concentrations of atmospheric CO_2 was compared against the measured A_{net} - c_i response curves.

ii) When used in the land-surface scheme, the coupled A_{net} - g_s model requires a single value for each of the photosynthetic parameters. Therefore, the average value of each photosynthetic parameter

derived from the A_{net} - c_i and A_{net} - P_{PFD} response curves, measured in well-watered trees, was used to calibrate the model, and model performance was assessed again. Model performance was also assessed using a default set of model parameter values as opposed to calibrated values.
iii) Using the calibration performed in step ii), the model configurations were validated against an independent data set of leaf-level A_{net} and g_s measured across the growing season under ambient atmospheric conditions, in healthy and water stressed top of canopy leaves of *P. nigra*.

2.6.3. Model configurations

The three different configurations of the JULES A_{net} - g_s model are summarised in Table 1. Model 1 is the photosynthesis sub-model currently used in JULES. Model 2 is equivalent to Model 1, but the transfer of c_i to c_c has been included according to Ethier & Livingston (2004). Model 3 uses the configuration of the Farquhar *et al*., (1980) photosynthesis model, which has been modified in the same manner as Model 2 to include the transfer of c_i to c_c. The main differences between the basic configuration of the Collatz *et al.,* (1991) model (Model 1 and Model 2) and the Farquhar *et al*., (1980) model (Model 3) is the description of the dependence of photosynthetic rate on light. The Farquhar *et al*., (1980) model uses an additional parameter, J_{max}, to determine the light limited rate of photosynthesis, whereas Model 1 and Model 2 use the Collatz et al., (1991) dependence on quantum yield. Model 2 and Model 3 use exponential temperature response functions for key temperature dependent parameters; K_o (Michaelis-Menton constant of Rubisco for O_2), K_c (Michaelis-Menton constant of Rubisco for CO_2), Γ* (chloroplastic CO_2 photocompensation point in the absence of mitochondrial respiration),V_{max}, J_{max}, R_d (dark respiration) and g_i. The temperature response functions used in Model 2 and Model 3 are those shown in Sharkey *et al*., (2007) and are reproduced here in equations 8 and 9. The Rubisco kinetic constants (K_o, K_c, Γ*) used in Model 2 and Model 3 are taken from Sharkey *et al*., (2007) and have been determined *in vivo* at c_c (Table 2). Because both Model 2 and Model 3 include g_i, they were parameterised with values of V_{max} estimated at c_c instead of c_i. Model 1 and uses Q_{10} temperature response functions as shown in Collatz *et al*., (1991) (see equation 7; Table 2). For all three models, calculation of the dark respiration rate and the triose-phosphate export limited rate of photosynthesis were the same, and followed the approach used in the Collatz *et al*., (1991) model.

2.6.4. Modelling photosynthesis with internal conductance to CO_2

Models 2 and 3 were modified to include the transfer of CO_2 from intercellular air spaces across the mesophyll cell wall and into the chloroplast. This followed the procedure of Ethier & Livingston (2004) who modified the biochemically based photosynthesis model of Farquhar *et al*., (1980) to

include this transfer. They developed a non-rectangular hyperbola version of the model that includes g_i to calculate both the CO_2- and light-limited rates of photosynthesis at the CO_2 concentration inside the chloroplast (c_c). This approach was taken in both Model 2 and Model 3. Under Rubsico limited conditions, the rate of photosynthesis can be determined at c_c by equation 1:

$$W_{carbc} = \frac{(c_c - \Gamma^*)V_{\max}}{c_c + K_c(1 + O_a / K_o)} - R_d \quad (1)$$

Where, W_{carbc} (µmol CO_2 m^{-2} s^{-1}) is the CO_2 - limited (or RuBP - saturated) CO_2 assimilation rate determined at c_c, c_c (Pa) is the chloroplastic CO_2 concentration and Γ^* (Pa) is the chloroplastic CO_2 photocompensation point in the absence of mitochondrial respiration. Substituting c_c with equation 2, where g_i (µmol CO_2 m^{-2} s^{-1} Pa^{-1}) is the internal CO_2 conductance transfer, gives a quadratic equation whose solution is the positive root (equation 3)

$$c_c = c_i - \frac{W_{carbc}}{g_i} \quad (2)$$

$$W_{carbc} = \frac{-b + \sqrt{b^2 - 4ac}}{2a}$$

where, $a = -1/g_i$

$$b = (V_{\max} - R_d)/g_i + c_i + K_c(1 + O_a / K_o)$$

$$c = R_d(c_i + K_c(1 + O_a / K_o)) - V_{\max}(c_i - \Gamma^*) \quad (3)$$

The light-limited rate of photosynthesis at c_c, W_{litec}, can be derived in a similar manner. Using the Farquhar *et al*., (1980) model (Model 3), W_{litec} is determined following equation 4:

$$W_{litec} = \frac{J/4(c_c - \Gamma^*)}{c_c + 2\Gamma^*} - R_d \quad (4)$$

Where, J (µmol e^- m^{-2} s^{-1}) is the rate of electron transport dependent on irradiance (I_{par}), given in equation 5 after Harley *et al*., (1992):

$$J = \frac{\alpha_{app} I_{par}}{\sqrt{1 + (\alpha_{app} I_{par} / J_{\max})^2}} \quad (5)$$

Where, J_{max} (µmol e^- m^{-2} s^{-1}) is the maximum electron transport rate, α_{app} (mol e^-/mol photons^{-1}) is the apparent quantum efficiency, and I_{par} (µmol m^{-2} s^{-1}) is the photosynthetically active radiation. In the Collatz *et al*., (1991) model, the description of the dependence of photosynthetic rate on light is dependent on the quantum yield, and is shown in equation 6 for determination at c_c:

$$W_{litec} = \frac{\alpha_{\text{int}} \omega I_{par} \left(c_c - \Gamma^*\right)}{c_c + 2\Gamma^*} - R_d \quad (6)$$

Where, ω is the leaf scattering coefficient for PAR (0.15) and α_{int} is the intrinsic quantum efficiency (mol CO_2 / mol^{-1} PAR). For simplicity we will call the first three terms on the top of equation 6 $J_{collatz}$ which describes the dependency of photosynthetic rate on available light in the Collatz *et al*., (1991) model. Consequently, like W_{carbc}, the light-limited CO_2 assimilation rate, W_{litec}, can be derived as outlined in equations 1 to 3 for Model 2 and Model 3 by replacing V_{max} with $J_{collatz}$ (Model 2) or with $J/4$ (Model 3), and $K_c(1 + O_a/K_o)$ with $2\Gamma^*$. The factor of four used in the Farquhar *et al*., (1980) model accounts for four electrons being required per carboxylation/oxygenation reaction.

2.6.5. Adjusting for temperature

In Model 1, temperature dependencies of the following parameters, R_d, V_{max}, g_i, K_o, K_c and Γ^* are described using a Q_{10} function shown in equation 7 (see Table 2).

$$f_T = f_{T25} Q_{10}^{0.1(T_c - 25)} \quad (7)$$

Where, f_{T25} is the parameter value at 25 °C and Q_{10} is the relative change in the parameter for a 10 °C change in temperature (Collatz et al., 1991). Exponential temperature response functions were used in Model 2 and Model 3. In this version of the model, the temperature dependence of V_{max}, J_{max}, R_d, K_c, K_o and Γ^* were each described by equation 8, (Harley et al., 1992; Sharkey et al., 2007);

$$Parameter = \exp\left(c - \Delta H_a / RT_c\right) \quad (8)$$

Where, c is a scaling constant, ΔH_a is an enthalpy of activation, R is the perfect gas constant (8.314 J mol^{-1} K^{-1}) and T_c is the leaf absolute temperature (°C). The temperature dependence for g_i used in Model 2 and Model 3 follows Bernacchi et al., (2002), and shown in equation 9 below:

$$Parameter = \frac{\exp\left(c - \Delta H_a / RT_c\right)}{1 + \exp\left[\left(\Delta ST_c - \Delta H_d\right) / RT_c\right]} \quad (9)$$

Where, ΔH_d is an enthalpy of deactivation and ΔS is an entropy term. The parameter values used are shown in Table 2.

2.7. Data

2.7.1. Model testing

The key photosynthetic parameters required by the three model configurations are shown in Table 1. Individual values of V_{max}, J_{max} and g_i inferred from the measured $A_{net} - c_i$ response curves were used to test the performance of the three model configurations (Table 3). V_{max} estimated without g_i (i.e. at c_i), was used in Model 1, whereas V_{max} estimated with g_i was used in Models 2 and 3. Additionally, Model 3 used values of J_{max} determined at c_c. The apparent quantum efficiency (α_{app}) describes the efficiency of light utilization in photosynthesis, and was inferred from the measured $A_{net} - P_{PFD}$ response curves. The intrinsic quantum efficiency (α_{int}), is similar to α_{app} but takes into account reflected and transmitted light and is therefore thought to be highly conserved across C_3 species (Long et al., 1993). Typical values for α_{int} range between 0.06 to 0.125 mol CO_2 mol^{-1}PAR (Collatz et al., 1991; Farquhar et al., 1980; Laisk et al., 2002; Lambers et al., 2008; Long et al., 1993). It is also suggested that there is a close relationship between α_{int} and F_v/F_m (the maximum potential quantum efficiency of photosystem II) as measured by chlorophyll fluorescence (Kao and Forseth, 1992). F_v/F_m was also measured in well-watered *P. nigra* trees over the same experimental period. Individual results are not reported, but F_v/F_m varied little over the course of the growing season, ranging between 0.072 - 0.08 mol CO_2 mol^{-1} PAR. The average of this range (0.076 mol CO_2 mol^{-1}PAR) was chosen as the value of α_{int} to use in both Model 1 and Model 2. F_0 (unit-less) and D_c (kg kg^{-1}) are additional model plant-specific parameters. F_0 is the c_i/c_a for specific humidity deficit in the canopy, and D_c is the critical humidity deficit. These parameters are not as readily measured, so it was necessary to tune these parameters to find suitable values. Each model was run in a Monte-Carlo simulation for 5000 iterations to find the parameter value that minimised the RMSD (root mean squared deviation) between modelled and observed A_{net}. The values of F_0 and D_c that minimised the RMSD were close to the default values for C_3 plants specified in the JULES documentation (Cox, 2001). It was observed that there was minimal sensitivity of simulated A_{net} to each of these parameters. The same values were used in all model configurations. At this stage, model testing was only performed with parameters from well watered trees, therefore the soil moisture stress factor (β) in the model was set to one (i.e. no soil moisture stress), (Cox et al., 1998).

2.7.2. Model Calibration

The leaf-level A_{net} - g_s model tested is integral to a land-surface scheme. This requires just one value for each parameter (V_{max}, J_{max}, g_i, α, F_0 and D_c). Therefore, the mean across the growing season from well-watered trees was used for each parameter. These values are shown in bold at the bottom of Table 3. Model 1was also used with a default parameter set for a broadleaf tree plant functional type (PFT) in the JULES model (JULES_def; V_{max} = 32.00, α_{int} = 0.076, F_0 = 0.875, D_c = 0.09). This was to assess the accuracy of modelled A_{net} when using default parameter values as opposed to calibrated parameters. This could not be done to compare the performance of Model 2 or Model 3 as default values for J_{max} and g_i were unknown.

2.7.3. Model Validation

Model validation was performed against measured leaf-level rates of A_{net} and g_s across the growing season in *P. nigra* trees under ambient environmental conditions and with imposed soil moisture stress. The soil moisture stress factor was calculated according to Cox *et al*., (1998).

2.7.4. Model assessment and statistical analyses

Observed data were plotted against their corresponding model-predicted values, model bias and goodness of fit was assessed based on the intercept, slope and coefficient of determination (r^2) of the optimal least squares regression line. Based on the recommendation of Piñeiro *et al*., (2008) all model assessments used regressions of observed (in the y-axis) vs. predicted (in the x-axis). The root mean squared deviation (RMSD) was also estimated.

Statistical analysis used a linear mixed effects model with the package *lme4* (Bates and Maechler, 2009) available in the statistical software *R2.10.1* (R2.10.1, 2009). The analysis tested main effects and interactions, with the random effect of block nested within treatment levels, and day of year. Significance of fixed effects were tested for using likelihood ratio tests (*LRT*) that use the chi-squared (x^2) distribution and maximum likelihood estimators (*MLE*) (Faraway, 2006).

2.7.5. Model driving data

Required meteorological driving variables were; leaf temperature (K), air pressure (Pa), PAR (W m^{-2}) and specific humidity (Q; kg kg^{-1}). Leaf temperature, air pressure and PAR were measured and

recorded by the IRGA at the time of measurement. Specific humidity (Q; kg kg^{-1}) was calculated using equation 10, where e_a is the actual vapour pressure (kPa) as measured by the IRGA:

$$Q = 0.622 e_a 0.01 \quad (10)$$

3. Results

3.1. Photosynthetic parameters

An effect of g_i on the estimate of V_{max} was detected in both well-watered and stressed trees ($x^2=15.7$, $p < 0.01$, $n = 50$). Estimates of V_{max} made assuming finite g_i resulted in significantly higher values of V_{max} (Fig 1a & b). Over the course of the growing season, in well-watered trees, V_{max} estimated at c_c ranged from 89.95 ± 21.7 µmol CO_2 m^{-2} s^{-1} to 106.84 ± 24.6 µmol CO_2 m^{-2} s^{-1} depending on measurement period, however, estimated at c_i, V_{max} ranged between 58.51 ± 12.2 µmol CO_2 m^{-2} s^{-1} to 70.64 ± 21.9 µmol CO_2 m^{-2} s^{-1}. In either case, the estimated values of V_{max} remained fairly constant for the duration of the growing season in control trees, with measurements falling well within the error of each other (Fig. 1a & b). During the measurement periods preceding a drought (Predrt.1 and Predrt.2 in Fig. 1), V_{max} estimated in both control and treatment trees were similar, falling well within the measurement error of each other (Fig. 1a & b). Drought led to a substantial decrease in estimated V_{max} compared to well-watered trees ($x^2=11.78$, $p < 0.01$, $n = 50$; Fig 1a & b). The mean of V_{max} estimated for stressed trees during the first drought period was 29.88 ± 13.7 µmol CO_2 m^{-2} s^{-1} (106.42 ± 4.9 µmol CO_2 m^{-2} s^{-1}) and 20.80 ± 5.8 µmol CO_2 m^{-2} s^{-1} (69.97 ± 5.9 µmol CO_2 m^{-2} s^{-1}) with and without g_i respectively (numbers in brackets indicate the corresponding value measured in control trees). During the second drought period this was 42.39 ± 3.9 µmol CO_2 m^{-2} s^{-1} (94.32 ± 15.4 µmol CO_2 m^{-2} s^{-1}) and 39.81 ± 2.9 µmol CO_2 m^{-2} s^{-1} (68.04 ± 3.8 µmol CO_2 m^{-2} s^{-1}) respectively. Mean soil moisture content during the first drought period (i.e. reported from the period when water was first withheld to just before re-watering) was 8.8 ± 6.8 % vol. with a minimum of 1.5 % vol., during the second drought period mean soil moisture content was 19.3 ± 7.9 % vol. with a minimum of 3.5 % vol (Fig. 2). It is notoriously difficult to impose a controlled drought, nevertheless, soil moisture content during both drought periods was sufficiently reduced to impact on estimates of V_{max} measured at both c_i and c_c (Fig. 2b). During the recovery period, V_{max} estimated in trees that were re-watered following drought was substantially higher than the control trees (Rec. in Fig. 1a & b). V_{max} estimated at c_c in trees recovering from drought was 230.14 ± 28.0 µmol CO_2 m^{-2} s^{-1} compared to 89.95 ± 21.7 µmol CO_2 m^{-2} s^{-1} measured in control trees.

There was no detectable effect of g_i on the estimate of J_{max}. As seen in Fig. 1c & d, estimates of J_{max} both with and without g_i were similar, for control trees these ranged between 121.84 ± 12.4 µmol CO_2 m^{-2} s^{-1} and 156.84 ± 48.7 µmol CO_2 m^{-2} s^{-1} when measured at c_c, and 108.18 ± 14.7 µmol CO_2 m^{-2} s^{-1} to 145.99 ± 50.0 µmol CO_2 m^{-2} s^{-1} when measured at c_i. Drought caused a significant decline of J_{max} ($x^2=12.70$, $p < 0.01$, $n = 50$). J_{max} in drought stressed trees declined to 47.87 ± 18.2 µmol CO_2 m^{-2} s^{-1} with g_i and 38.55 ± 11.4 µmol CO_2 m^{-2} s^{-1} without g_i during the first drought period, and 53.35 ± 5.3 µmol CO_2 m^{-2} s^{-1} and 51.81 ± 4.5 µmol CO_2 m^{-2} s^{-1} respectively during the second drought period. Similar to V_{max}, it is likely that J_{max} declined less during the second drought period because the reduction is soil moisture content was less severe (Fig. 2). As stressed trees were re-watered following the first drought, J_{max} measured in these trees was significantly higher compared to control trees. In stressed trees recovering from drought, J_{max} was 260.21 ± 14.0 µmol CO_2 m^{-2} s^{-1} compared to 116.09 ± 15.3 µmol CO_2 m^{-2} s^{-1} (with g_i), and 239.65 ± 17.2 µmol CO_2 m^{-2} s^{-1} compared to 108.18 ± 14.7 µmol CO_2 m^{-2} s^{-1} (without g_i).

Internal conductance to CO_2 (g_i) declined with water stress ($x^2=18.4$, $p < 0.01$, $n = 25$; Fig. 1e and see Fig. 2b). In control trees however, g_i remained consistent over the course of the growing season, with no detectable differences between the different measurement periods. In control *P. nigra* trees, g_i ranged between 1.75 ± 0.3 µmol m^{-2} s^{-1} Pa^{-1} to 2.55 ± 0.8 µmol m^{-2} s^{-1} Pa^{-1} (Fig. 1e). In droughted trees, g_i declined to 0.41 ± 0.01 µmol m^{-2} s^{-1} Pa^{-1} to 0.60 ± 0.07 µmol m^{-2} s^{-1} Pa^{-1} during the first and second drought periods respectively. In trees recovering from water stress, g_i was higher (3.38 ± 0.1µmol m^{-2} s^{-1} Pa^{-1}), but this was within the measurement error of g_i measured in control trees (2.55 ± 0.8µmol m^{-2} s^{-1} Pa^{-1}; Fig. 1e).

3.2. Model testing

All model configurations simulated observed rates of A_{net} with high accuracy (Fig. 3a-c). Model 1 was seen to marginally over predict at low values of A_{net} and under predict at high rates (Fig. 3a). Both the intercept and slope of the regression line were found to be significantly different from zero and one respectively (Table 4). Although the bias in the relationship was small, as shown by the 95% confidence intervals (CIs) surrounding the slope and intercept. Further, the coefficient of determination (r^2) was high (0.98), and the RMSD low (1.68 µmol CO_2 m^{-2} s^{-1}; Table 4). Model 2 reduced the accuracy of simulated A_{net} compared to Model 1 (Fig. 3b). The r^2 declined to 0.93 and the RMSD increased to 5.86 µmol CO_2 m^{-2} s^{-1}. Model 2 showed a pronounced bias to over-estimate A_{net} that increased with increasing A_{net}. The scatter around the model regression line was much greater, with larger CIs around the slope and intercept of the line (Table 4). No significant improvement in modelled A_{net} was seen with Model 3 compared to Model 1 (Fig. 3c). Although the r^2 were identical,

Model 3 generated a marginal increase in the RMSD (1.71µmol CO_2 m^{-2} s^{-1}) compared to Model 1. Model 3 showed a similar bias in predicted A_{net} to Model 1, over predicting at low values and under predicting at high values of A_{net} (Table 4). Model 3, however, improved the accuracy of simulated A_{net} compared to Model 2.

3.3. Model calibration

Model 1 maintained a good fit to the observed data, the r^2 remained reasonably high at 0.76 (Fig. 3d), and the RMSD was 5.34µmol CO_2 m^{-2} s^{-1} (Table 4). The regression model line was not significantly different to the 1:1 line, however, the CIs surrounding the slope and intercept were substantially larger compared to the model testing stage. This suggests greater uncertainty in the fit between observed and modelled data. Model 2 generated a slight decrease in the accuracy of predicted A_{net} (Fig. 3e). Although the r^2 increased to 0.80, the RMSD also increased to 7.18µmol CO_2 m^{-2} s^{-1}, which is substantially larger than either Model 1 or Model 3. There was also significant bias in the model to over-estimate A_{net} which was less pronounced in Model 1 or Model 3 (Table 4; Fig. 3). The performance of Model 3 was almost identical to Model 1 (Fig. 3f). The r^2 was 0.76 and the RMSD only marginally increased to 5.35 µmol CO_2 m^{-2} s^{-1} (Table 4). Also, similar to Model 1, the regression line was not significantly different to the 1:1 line, and the CIs surrounding this line were similar. Compared to Model 2, Model 3 increased the accuracy of predicted A_{net}. In each model configuration, the single parameter set clearly maintained a high level of accuracy of simulated A_{net}, however there was noticeably more variation surrounding the model predicted values compared to the use of 'curve-specific' parameter values. This is to be expected, as each model was simulating observations from across the growing season with the use of a single calibrated parameter set, and it was seen that values inferred from each A_{net} - c_i and A_{net} - P_{PFD} curve varied across the growing season. Given the sensitivity of modelled A_{net} to V_{max} in particular, an exact match between the observed and modelled data could never be expected given the seasonal variation.

Comparison of Model 1 and Model 1_{def} (Table 4) shows the increased accuracy of using calibrated parameters as opposed to default model values. Use of the latter led to substantial under prediction of A_{net}. The RMSD was increased from 5.34µmol CO_2 m^{-2} s^{-1} to 9.42µmol CO_2 m^{-2} s^{-1} (Table 4). These simulations using the default parameter values highlight the sensitivity of simulated A_{net} to the photosynthetic parameter V_{max}. Values of α_{int}, F_0 and D_c changed marginally between the default values and calibrated parameter sets. Additionally, in a previous Monte Carlo experiment to determine suitable values for D_c and F_0, it was seen that A_{net} displayed little sensitivity to these parameters. V_{max}, however, changed significantly between simulations, with the calibrated values

being more than double the default value. Therefore, correct calibration of V_{max} is key to improving predictions of leaf-level A_{net}.

3.4. Model validation

The accuracy of Model 1, the simplest model, and Model 3, the best performing 'alternative' model, were validated in this section.

3.4.1. Photosynthesis

The accuracy of simulated A_{net} was improved by Model 1 compared to Model 3 (Fig. 3g & i). Model 1 is the JULES model in its original configuration and is the simplest model. The improvement in accuracy seen with Model 1 was slight, nevertheless, r^2 increased from 0.72 (Model 3) to 0.77 (Model 1). The RMSD decreased from 3.91 µmol CO_2 m^{-2} s^{-1} (Model 3) to 3.36 µmol CO_2 m^{-2} s^{-1} (Model 1; Table 4). Both models suggested bias in model predictions, both the regression line slope and intercept were different to the 1:1 line suggesting a tendency to over predict A_{net} at higher values and under-predict at lower values (Table 4). Although this appears slightly less pronounced in Model 1, as the 95% CI surrounding the intercept in marginally smaller for Model 1.

3.4.2. Stomatal conductance

The accuracy of simulated g_s was marginally improved in Model 3 (Fig. 3h & j). The r^2 was higher in Model 3 (0.86) than Model 1 (0.82), and the RMSD was lower in Model 3 (58.23 mmol H_2O m^{-2} s^{-1}) than Model 1 (65.45 mmol H_2O m^{-2} s^{-1}). In both models, the regression model slope was significantly different to one. The intercepts were not different to zero, however the CI surrounding the intercept was smaller in Model 3. Nevertheless, in both models, the accuracy of simulated g_s was high.

4. Discussion

4.1. Photosynthetic parameters

In this work, estimates of V_{max} made under the assumption of infinite g_i were significantly lower than V_{max} estimated assuming finite g_i. Therefore, in fast growing poplar genotypes, such as *P. nigra* used in this study, the assumption that internal CO_2 transfer is infinitely large as to have a negligible impact on the drawdown of CO_2 from c_i to c_c is invalid. Under well-watered conditions, values of

518 V_{max} calculated from A_{net} - c_c curves were, on average, 52 % higher than values calculated from A_{net} -
519 c_i curves in *P. nigra* SRC trees. The differences between c_i and c_c based estimates of V_{max} in this
520 poplar genotype are large. There are no comparable studies of poplars in the literature, but Niinemets
521 *et al*., (2009) reported V_{max} calculated on a c_c basis was 25 % higher than on a c_i basis in young fully
522 mature leaves of field-grown olive trees. Bown *et al*., (2009) found mean values of V_{max} calculated
523 on a c_c basis were 15.4 % higher in pot grown *Pinus radiata* trees. Both these studies show smaller
524 differences than in this study. Manter and Kerrigan (2004), however, reported differences in c_i versus
525 c_c based estimates of V_{max} for 19 woody tree species that were very wide ranging, from -1.6%
526 (*Quercus garryana*) to +92.1% (*Abies concolor*). The results from this study fall within the mid
527 range of these values. Similar to these studies, this work highlights the impact g_i has on estimates of
528 this important photosynthetic parameter. In contrast, accounting for g_i did not result in significantly
529 higher estimates of J_{max} in this study. Similarly, other studies have found that differences in J_{max}
530 calculated on a c_i or c_c basis are small (Flexas et al., 2007b; Niinemets et al., 2009; Warren, 2008).
531
532 In this study, values of g_i for well-watered *P. nigra* trees ranged between 1.12 – 3.74 μmol m^{-2} s^{-1} Pa^{-1}
533 , Flexas *et al*., (2008) report a range of g_i from literature measured in *Populus* species of between
534 0.4 to 5.0 μmol m^{-2} s^{-1} Pa^{-1}, whilst this range is very large, it at least confirms that g_i measured in this
535 study falls well within this. The drought induced decline in g_i was significant, indicating a substantial
536 contribution of this diffusive limitation to photosynthetic carbon gain during the two periods of water
537 stress. During drought, g_i declined to 0.41 ± 0.01 μmol m^{-2} s^{-1} Pa^{-1} and 0.60 ± 0.07 μmol m^{-2} s^{-1} Pa^{-1}
538 in *P. nigra* trees during the first and second drought period respectively. Although values of g_i
539 reported in this study are relatively high, there is noticeable variation in the measurements.
540 Consequently, at times it is possible g_i may be limiting to photosynthesis even under well-watered
541 conditions. This identifies a potential target for breeding programmes to improve yields and water-
542 use efficiency (Centritto et al., 2009).
543
544 Unlike the work of Galmés et al., (2007), this study found that values of V_{max} and J_{max} in re-watered
545 trees following the first drought period were almost two-fold higher than those of control trees.
546 Poplar species are typically pioneers of riparian ecosystems, as such, many poplar species are
547 notoriously susceptible to, and display limited sensitivity to drought (Hall and Allen, 1997; Monclus
548 et al., 2006). In this study, A_{net} and g_s in *P. nigra* trees only declined once the soil moisture deficit
549 was below an apparent critical threshold of soil moisture content (11-18 % vol.). This threshold
550 response has been observed in other genotypes of poplar (Hall and Allen, 1997). In addition to
551 reduced A_{net} and g_s, the leaves of *P. nigra* trees in this study were observed to yellow, this was
552 followed by leaf shedding. This is a common mechanism of acclimation to drought conditions in fast
553 growing species, and before leaf senescence, nitrogen is assimilated out of leaves (Lambers et al.,

554 2008). There is a strong correlation between leaf nitrogen content and photosynthetic capacity since
555 the proteins of the thylakoids and Calvin cycle (e.g. Rubisco, the enzyme involved in CO_2 fixation)
556 represent the majority of leaf nitrogen (Evans, 1989). Consequently, depletion of leaf nitrogen as a
557 result of drought leads to photosynthetic down-regulation resulting from necessary adjustments to the
558 biochemical photosynthetic capacity. During drought, Rubisco content and/or activity has been
559 observed to decline as a result of either reduced leaf nitrogen content and/or different partitioning of
560 leaf nitrogen among photosynthetic enzymes (Bota et al., 2004; Castrillo et al., 2001; Grassi and
561 Magnani, 2005; Parry et al., 2002; Tezera et al., 2002) leading to a decline in V_{max} and J_{max}. Large
562 increases in biochemical photosynthetic capacity upon re-watering may result from the allocation of
563 assimilated nitrogen back to the leaves, or partitioning of more nitrogen to photosynthetic enzymes
564 such as Rubisco, to maximise growth once favourable environmental conditions return. This strategy
565 may be symptomatic of the life strategy of this poplar species as a fast-growing pioneer.
566
567 The observed decline in V_{max} and J_{max} during drought was apparent when measured at both c_c and c_i,
568 suggesting there is a biochemical limitation to photosynthetic capacity during periods of water stress.
569 Additionally, the up-regulation of these parameters upon re-watering suggests that V_{max} and J_{max} are
570 highly plastic. This has implications for land-surface modelling and the representation of drought
571 within these models. Currently in the JULES A_{net} - g_s model, water stress effects on A_{net} and g_s are
572 accounted for by applying a normalised soil moisture dependent function to A_{net} directly (Best et al.,
573 2011). The potential (i.e. non water stressed) rate of A_{net} is calculated and then modified by the soil
574 moisture stress function. The rate of g_s in response to water stress is then modified accordingly, and
575 is derived from a semi-empirical function that relates g_s to modelled A_{net} and intercellular/
576 atmospheric CO_2 concentration (Best et al., 2011). However, the results of this work suggest it may
577 be more appropriate to apply the soil moisture stress function directly to one or more parameters in
578 the photosynthesis model itself, such as V_{max} and J_{max}, to better represent this biochemical limitation
579 to photosynthetic capacity during drought.
580
581 The measured reduction in V_{max} and J_{max} clearly shows there was a biochemical limitation to
582 photosynthesis during drought in *P. nigra* trees. However, the threshold function that described the
583 decline in g_s with increasing water stress in *P. nigra* trees in this study was mirrored by A_{net}, which
584 clearly suggests a stomatal limitation to photosynthetic carbon gain. Further, the decline in g_i with
585 drought suggests an additional diffusional limitation. The consensus in the literature on the main
586 processes governing photosynthetic limitation during drought is diffusional processes at mild to
587 moderate drought, and biochemical processes during severe water stress (Flexas et al., 2006; Flexas
588 et al., 2004a; Flexas et al., 2008; Grassi and Magnani, 2005; Lawlor and Cornic, 2002). The current
589 representation of water stress in the JULES A_{net} - g_s model uses a linear function to model the

response of A_{net} and g_s to drought, which is evidently not appropriate for all species. Moreover, the results of this work and the literature suggest that future work should consider modelling drought through biochemical and diffusional controls, since it is the sum of both these processes that determine water stressed A_{net}. Initial work by Egea et al., (2011) in this area demonstrated that in the coupled A_{net} - g_s model used in their work, it was necessary to combine both diffusional and biochemical limitations of A_{net} to accurately capture observed functional relationships between A_{net} and g_s in response to drought.

For the purposes of this work, V_{max} was parameterised directly using field measurements of V_{max} from *P. nigra* trees. Currently, in the JULES model, V_{max} can be parameterised with a distribution of leaf nitrogen (N) that allows V_{max} to decrease from top to bottom of the canopy (see Eq. (28) from Clark et al., 2011). However, currently, leaf N, and hence V_{max}, does not vary temporally. This means that the high plasticity observed in V_{max} in this study, when stressed trees were re-watered, would be difficult to represent in the model. In addition, other studies have shown that V_{max} decreases over the course of the growing season (Grassi et al., 2005; Niinemets et al., 1999; Wilson et al., 2001), which again is not possible to simulate without temporal variation in V_{max}, or leaf N concentration. It has been shown that modelled seasonal trends in carbon fluxes are explained best with a temporally varying V_{max} (Wang et al., 2004; Wilson et al., 2001). Therefore, a time-varying V_{max} would allow for greater plasticity in this parameter as is observed in the field. It may be possible to link water stress effects on plant A_{net} and g_s to changes in leaf N concentration, although this would likely require a prognostic model of nitrogen availability and uptake by plants. Nevertheless, results from this work and the literature suggest that the photosynthetic capacity of plants changes with time and environmental conditions, which indicates there should be greater flexibility in the temporal parameterisation of V_{max}. This may be possible to do with respect to the different plant functional types (PFTs) used in land-surface models, however, comparing the large increase in V_{max} upon re-watering observed in this study with the results of Galmés et al., (2007) shows that there is significant variation between species in the way this parameter responds to water stress and its alleviation.

4.2. Does inclusion of g_i in a coupled A_{net} - g_s model improve the accuracy of simulated A_{net} and g_s?

The results of model testing, calibration and validation from this work suggest there is no significant improvement in the accuracy of modelled A_{net} from the inclusion of g_i to necessitate the addition of this process to the JULES A_{net} - g_s model parameterisation (Table 4; Fig. 3). Testing, calibration and validation of the three model configurations agreed and showed that the performance of Model 1 (no

626 g_i) and Model 3 (with g_i), were very similar. Both model configurations shared high r^2 and low
627 RMSD (Table 4). In this work, g_i was included in model configurations 2 and 3 as a constant, using
628 the mean g_i value measured in unstressed *P. nigra* trees over the course of the experimental period.
629 Simulated A_{net} and g_s values in Model 1 used an 'apparent' value of V_{max} (i.e. determined at c_i),
630 whereas Model 2 and 3 used a 'true' value of V_{max} (i.e. determined at c_c). The true V_{max} value is
631 estimated by explicitly modelling the extra diffusional pathway from c_i to c_c, whereas the apparent
632 value inherently includes this information about g_i. Therefore, including g_i in the model
633 configurations did not have a large impact on the accuracy of modelled A_{net} and g_s in the coupled
634 model since the value of V_{max} used in each model configuration compensated for the
635 presence/absence of this additional pathway.
636
637 V_{max} is generally regarded as a good indicator of photosynthetic capacity and is considered a directly
638 transferable parameter to calibrate models of ecosystem carbon exchange. However, given the
639 difference between estimates of V_{max} determined at either c_c or c_i, the assumed transferability of this
640 parameter from measurements to models and between models is not so straightforward. It must be
641 ensured that values of V_{max} used in carbon exchange models are correct for the assumptions
642 underlying the model (i.e. determination of photosynthesis on a c_i or c_c basis). If, for example, a true
643 V_{max} value were used to parameterise a photosynthesis model that calculated A_{net} at c_i, it is likely that
644 A_{net} would be grossly over-estimated because of the significantly higher value of V_{max}, and the lack of
645 explicit representation of the c_i to c_c CO_2 transfer. This would likely propagate into errors in the
646 prediction of ecosystem NPP at the larger scale.
647
648 Simulated A_{net} using a default model set of parameter values highlighted the sensitivity of simulated
649 A_{net} to V_{max}. In this simulation, the accuracy of predicted A_{net} was greatly reduced; the RMSD was
650 almost two times higher the RMSD from model configurations 1 to 3 which used a calibrated value
651 of V_{max} for *P. nigra* (Table 4). This high sensitivity to V_{max} again emphasises the importance of
652 correctly matching values of V_{max} (i.e. true or apparent) to the correct assumptions of the
653 photosynthesis model. Moreover, however, it suggests that the uncertainty surrounding values of
654 V_{max} used to parameterise land-surface models potentially has a much greater impact on the
655 simulation of A_{net} than other fine-scale leaf-level processes such as internal CO_2 transfer. Recent
656 work by Bonan et al., (2011) on improving canopy processes in the Community Land Model version
657 4 (CLM4) concludes that uncertainty in the parameter V_{max} produces effects of comparable
658 magnitude as model structural errors, and that currently, V_{max} remains a poorly constrained, model-
659 dependent parameter.
660

Represented as a constant, unstressed, value of g_i in different configurations of the coupled A_{net} - g_s model, the inclusion of g_i to simulate the extra diffusional pathway of CO_2 from c_i to c_c during photosynthesis did not improve the accuracy of simulated A_{net} and g_s. Given the current limited understanding of g_i, it was necessary to take such an approach. Few models simulating whole plant carbon exchange consider the internal transfer of CO_2 as part of their parameterisation. The ISBA-Ags land-surface model (Calvet et al., 1998), C-TESSEL surface exchange scheme (Voogt et al., 2005), and the SPA model (Williams et al., 1996) are the few examples of models that do include g_i. In these models, g_i is also parameterised as a constant value. Similar to g_s, however, g_i is known to respond to changing environmental conditions in the long (days/weeks) and short (minutes) term (Flexas et al., 2008; Warren, 2008). A process-based implementation of g_i may therefore be more desirable, currently, however, there are significant research gaps that would make this difficult. These include the variation in g_i with temperature, the response of g_i to light and vapour pressure deficit, and scaling g_i within the canopy (Bernacchi et al., 2002; Flexas et al., 2008; Niinemets et al., 2006; Warren, 2008; Warren and Adams, 2006; Warren and Dreyer, 2006). Consequently, greater understanding of the interaction of g_i with its environment is needed before a truly process-based approach can be used to model this additional CO_2 pathway. Nevertheless, this work contributes to our understanding of the impact of g_i in land-surface modelling, and raises further issues that may be of equal importance to address before consideration of additional fine-scale leaf-level processes such as g_i. These include the uncertainty surrounding values of V_{max} used in land-surface models, and the representation of water stress effects on vegetation within such models.

Acknowledgements:

We would like to thank Lina Mercado, Martin De Kauwe and two anonymous reviewers for reading and improving drafts of this manuscript. We would also like to acknowledge the time and help from Lina Mercado given during the analysis of this work. We would like to thank Mike Morecroft for advice on the experimental design, and John Krebs field station, Oxfordshire for supporting our field work. We would like to thank Mike Cotton at Southampton University, John Fuller, Richard Hailstone and Julie Hailstone for their assistance preparing and setting up the experimental plant material. RJO was supported by a research studentship from the Natural Environment Research Council (no. NER/S/A/2006/14314).

References

Bates, D. and Maechler, M., 2009. *lme4*: Linear mixed-effects models using S4 classes. R package version 0.999375-32. In: http://CRAN.R-project.org/package=lme4 (Editor).

Bernacchi, C., Portis, A.R., Nakano, H., von Caemmerer, S. and Long, S.P., 2002. Temperature response of mesophyll conductance. Implications for the determination of Rubisco enzyme kinetics and for limitations to photosynthesis *in vivo*. Plant Physiology, 130: 1992-1998.

Bernacchi, C.J. et al., 2003. Photosynthesis and stomatal conductance responses of poplars to free-air CO_2 enrichment (PopFACE) during the first growth cycle and immediately following coppice. New Phytologist, 159: 609-621.

Best, M.J. et al., 2011. The Joint UK Land Environment Simulator (JULES), Model description - Part 1: Energy and water fluxes. Geoscientific Model Development Discussions, 4: 595-640.

Bonan, G.B. et al., 2011. Improving canopy processes in the Community Land Model version 4 (CLM4) using global flux fields empirically inferred from FLUXNET data. Journal of Geophysical Research, 116: 1-22.

Bota, J., Medrano, H. and Flexas, J., 2004. Is photosynthesis limited by decreased Rubisco activity and RuBP content under progressive water stress? New Phytologist, 162(3): 671-681.

Bown, H.E., Watt, M.S., Mason, E.G., Clinton, P.W. and Whitehead, D., 2009. The influence of nitrogen and phosphorus supply and genotype on mesophyll conductance limitations to photosynthesis in *Pinus radiata*. Tree Physiology(1-0).

Calvet, J.C. et al., 1998. An interactive vegetation SVAT model tested against data from six contrasting sites. Agricultural and forest meteorology, 92: 73-95.

Castrillo, M., Fernandez, D., Calcagno, A.M., Trujillo, I. and Guenni, L., 2001. Responses of ribulose-1,5-bisphosphate carboxylase, protein content, and stomatal conductance to water deficit in maize, tomato, and bean. Photosynthetica, 39: 221-226.

Centritto, M., Lauteri, M., Monteverdi, M.C. and Serraj, R., 2009. Leaf gas exchange, carbon isotope discrimination, and grain yield in contrasting rice genotypes subjected to water deficits during the reproductive stage. Journal of Experimental Botany, 60(8): 2325-2339.

Centritto, M., Loreto, F. and Chartzoulakis, K., 2003. The use of low CO_2 to estimate diffusional and non-diffusional limitations of photosynthetic capacity of salt-stressed olive saplings. Plant, Cell & Environment, 26(4): 585-594.

Clark, D.B. et al., 2011. The Joint UK Land Environment Simulator (JULES), Model description - Part 2: Carbon fluxes and vegetation. Geoscientific Model Development Discussions, 4: 641-688.

Collatz, G.J., Ball, J.T., Grivet, C. and Berry, J.A., 1991. Physiological and environmental regulation of stomatal conductance, photosynthesis and transpiration: A model that includes a laminar boundary layer. Agricultural and Forest Meteorology, 54: 107-136.

Collatz, G.J., Ribas-Carbo, M. and Berry, J.A., 1992. A coupleed photosynthesis-stomatal conductance model for leaves of C_4 plants. Australian Journal of Plant Physiology, 19: 519-538.

Cox, P.M., 2001. Description of the TRIFFID dynamic global vegetation model. Hadley Centre technical note 24.

Cox, P.M., Huntingford, C. and Harding, R.J., 1998. A canopy conductance and phtosynthesis model for use in a GCM land surface scheme. Journal of Hydrology, 212-213: 79-94.

During, H., 2003. Stomatal and mesophyll conductances control CO_2 transfer to chloroplasts in leaves of grapevine (*Vitis vinifera L.*). Vitis, 42: 65-68.

Egea, G., Verhoef, A. and Vidale, P.L., 2011. Towards an improved and more flexible representation of water stress in coupled photosynthesis-stomatal conductance models. Agricultural and Forest Meteorology, 151(10): 1370-1384.

Ethier, G.J. and Livingston, N.J., 2004. On the need to incorporate sensitivity to CO_2 transfer conductance into the Farquhar-von Caemmerer-Berry leaf photosynthesis model. Plant, Cell & Environment, 27: 137-153.

Evans, J.R., 1989. Photosynthesis and nitrogen relationships in leaves of C3 plants. Oecologia, 78: 9-19.

Faraway, J., J., 2006. Extending the linear model with R: generalized linear, mixed effects and nonparametric regression models. Tests in Statistical Science. Chapman & Hall.

748 Farquhar, G.D., Von Caemmerer, S. and Berry, J.A., 1980. A biochemical model of photosynthetic CO_2
749 assimilation in leaves of C_3 species. Planta, 149: 78-90.
750 Flexas, J., Bota, J., Galmes, J., Medrano, H. and Ribas-Carbo, M., 2006. Keeping a positive carbon balance
751 under adverse conditions: responses of photosynthesis and respiration to water stress. Physiologia
752 Plantarum, 127(3): 343-352.
753 Flexas, J., Bota, J., Loreto, F., Cornic, G. and Sharkey, T.D., 2004a. Diffusive and metabolic limitations to
754 photosynthesis under drought and salinity in C_3 plants. Plant Biology, 6: 269-279.
755 Flexas, J. et al., 2007a. Rapid variations of mesophyll conductance in response to changes in CO_2
756 concentration around leaves. Plant, Cell & Environment, 30: 1284-1298.
757 Flexas, J., Escalona, J.M., Sampol, B. and Medrano, H., 2002. Effects of drought on phtosynthesis in
758 grapevines under field conditions: an evaluation of stomatal and mesophyll limitations. Functional
759 Plant Biology, 29: 461-471.
760 Flexas, J., Ribas-Carbo, M., Diaz-Espejo, A., Galmes, J. and Medrano, H., 2007b. Mesophyll conductance to
761 CO_2: current knowledge and future prospects. Plant, Cell & Environment, 31: 602-621.
762 Flexas, J., Ribas-Carbo, M., Diaz-Espejo, A., Galmes, J. and Medrano, H., 2008. Mesophyll conductance to
763 CO_2: current knowledge and future prospects. Plant, Cell & Environment, 31: 602-621.
764 Galmés, J., Medrano, H. and Flexas, J., 2007. Photosynthetic limitations in response to water stress and
765 recovery in Mediterranean plants with different growth forms. New Phytologist, 175(1): 81-93.
766 Grassi, G. and Magnani, F., 2005. Stomatal, mesophyll conductance and biochemical limitations to
767 photosynthesis as affected by drought and leaf ontogeny in ash and oak trees. Plant, Cell &
768 Environment, 28(7): 834-849.
769 Grassi, G., Vicinelli, E., Ponti, F., Cantoni, L. and Magnani, F., 2005. Seasonal and interannual variability of
770 photosynthetic capacity in relation to leaf nitrogen in a deciduous forest plantation in northern Italy.
771 Tree Physiology, 25: 349-360.
772 Hall, R.L. and Allen, S.J., 1997. Water use of poplar clones grown as short-rotation coppice at two sites in the
773 United Kingdom. Aspects of Applied Biology, 49: 163-171.
774 Harley, P.C., Thomas, R.B., Reynolds, J.F. and Strain, B.R., 1992. Modelling photosynthesis of cotton grown in
775 elevated CO_2. Plant , Cell and Environment, 15: 271-282.
776 Hughes, J.K., Lloyd, A.J., Huntingford, C., Finch, J.W. and Harding, R.J., 2010. The impact of extensive planting
777 of *Miscanthus* as an energy crop on future CO_2 atmospheric concentrations. Global Change Biology
778 Bioenergy, 2: 79-88.
779 Kao, W.Y. and Forseth, I.N., 1992. Diurnal leaf movement, chlorophyll fluorescence and carbon assimilation
780 in soy-bean grown under different nitrogen and water availabilities. Plant , Cell and Environment, 15:
781 703-710.
782 Laisk, A. et al., 2002. A computer-operated routine of gas exchange and optical measurements to diagnose
783 photosynthetic apparatus in leaves. Plant , Cell and Environment, 25: 923-943.
784 Lambers, H., Chapin III, F.S. and Pons, T.L., 2008. Plant Physiological Ecology. Springer, New York.
785 Lawlor, D.W. and Cornic, G., 2002. Photosynthetic carbon assimilation and associated metabolism in relation
786 to water deficits in higher plants. Plant , Cell and Environment, 25: 275-294.
787 Long, S.P. and Bernacchi, C.J., 2003. Gas exchange measurements, what can they tell us about the underlying
788 limitations to photosynthesis? Procedures and sources of error. J. Exp. Bot., 54(392): 2393-2401.
789 Long, S.P., Postl, W.F. and Bolhar-Noedenkampf, H.R., 1993. Quantum yields for uptake of carbon dioxide in
790 C_3 vascular plants of contrasting habitats and taxonomic groupings. Planta, 189: 226-234.
791 Manter, D.K. and Kerrigan, J., 2004. A/C_i curve analysis across a range of woody plant species: influence of
792 regression analysis parameters and mesophyll conductance. J. Exp. Bot., 55(408): 2581-2588.
793 Monclus, R. et al., 2006. Impact of drought on productivity and water use efficiency in 29 genotypes of
794 *Populus deltoides* x *Populus nigra*. New Phytologist, 169(4): 765-777.
795 Niinemets, Ü., Bilger, W., Kull, O. and Tenhunen, J.D., 1999. Responses of foliar photosynthetic electron
796 transport, pigment stoichiometry, and stomatal conductance to interacting environmental factors in
797 a mixed species forest canopy. Tree Physiology, 19: 839-852.
798 Niinemets, Ü., Cescatti, A., Rodeghiero, M. and Tosens, T., 2006. Complex adjustments of photosynthetic
799 potentials and internal diffusion conductance to current and previous light availabilities and leaf age
800 in Mediterranean evergreen species *Quercus ilex*. Plant, Cell and Environment, 29(6): 1159-1178.

Niinemets, Ü., Diaz-Espejo, A., Flexas, J., Galmes, J. and Warren, C.R., 2009. Importance of mesophyll diffusion conductance in estimation of plant photosynthesis in the field. Journal of Experimental Botany, 60(8): 2271-2282.
Parry, M.A., Andralojc, P.J., Khan, S., Lea, P.J. and Keys, A.J., 2002. Rubisco activity: effects of drought stress. Annals of Botany, 89: 833-839.
Parsons, R. and Ogston, S.A., 1998. Photosynthesis Assistant - Windows software for analysis of photosynthesis. Dundee Scientific, Dundee, Scotland.
Piñeiro, G., Perelman, S., Guerschman, J.P. and Paruelo, J.M., 2008. How to evaluate models: Observed vs. predicted or predicted vs. observed? Ecologicla Modelling, 216: 316-322.
Pons, T.L. et al., 2009. Estimating mesophyll conductance to CO_2: methodology, potential errors, and recommendations. Journal of Experimental Botany, 60(8): 2217-2234.
Prioul, J.L. and Chartier, P., 1977. Partitioning of transfer and carboxylation components of intracellula resistance to photosynthetic CO_2 fixation: A critical analysis of the methods used. Annals of Botany, 41: 789-800.
R2.10.1, 2009. R Core Development Team: A language and environment for statistical computing. In: V. R Foundation for Statistical Computing, Austria. (Editor), ISBN 3-900051-07-0, URL http://www.R-project.org.
Sharkey, T.D., Bernacchi, C.J., Farquhar, G.D. and Singsaas, E.L., 2007. Fitting photosynthetic carbon dioxide response curves for C_3 leaves. Plant , Cell and Environment, 30: 1035-1040.
Tezera, W., Mitchell, V.J., Driscoll, S.D. and Lawlor, D.W., 2002. Effects of water deficit and its interaction with CO_2 supply on the biochemistry and physiology of photosynthesis in sunflower. Journal of experimental Botany, 53: 1781-1791.
Vanloocke, A., Bernacchi, C.J. and Twines, T.E., 2010. The impacts of *Miscanthus* x *giganteus* production on the Midwest US hydrologic cycle. Global Change Biology Bioenergy, 2: 180-191.
Voogt, M.H., Van den Hurk, B.J.J.M. and Jacobs, C.M.J., 2005. The ECMWF land surface scheme extended with a photosynthesis and LAI module tested for a coniferous forest site.
Wang, Q. et al., 2004. Simulation and scaling of temporal variation in gross primary production for coniferous and deciduous temperate forests. Global Change Biology, 10(1): 37-51.
Warren, C.R., 2008. Stand aside stomata, another actor deserves centre stage: the forgotten role of the internal conductance to CO_2 transfer. Journal of Experimental Botany, 59(7): 1475-1487.
Warren, C.R. and Adams, M.A., 2006. Internal conductance does not scale with photosynthetic capacity: implications for carbon isotope discrimination and the economics of water and N use in photosynthesis. Plant, Cell & Environment, 29: 192-201.
Warren, C.R. and Dreyer, E., 2006. Temperature response of photosynthesis and internal conductance to CO_2: results from two independent approaches. Journal of Experimental Botany, 57(12): 3057-3067.
Warren, C.R., Livingston, N.J. and Turpin, D.H., 2004. Water stress decreases the transfer conductance of Douglas-fir (*Pseudotsuga menziesii*) seedlings. Tree Physiology, 24: 971-979.
Williams, M. et al., 1996. Modelling the soil-plant-atmosphere continuum in a *Quercus-Acer* stand at Harvard Forest: the regulation of stomatal conductance by light, nitrogen and soil/plant hydraulic properties. Plant, Cell & Environment, 19: 911-927.
Wilson, K.B., Baldocchi, D.D. and Hanson, P.J., 2001. Leaf age affects the seasonal pattern of photosynthetic capacityand net ecosystem exchange of carbon in a deciduous forest. Plant, Cell & Environment, 24(6): 571-583.

	Model 1	Model 2	Model 3
V_{max}	x	x	x
α (int/app)	x (int)	x (int)	x (app)
g_i	n/a	x	x
J_{max}	n/a	n/a	x
F_0	x	x	x
D_c	x	x	x
Temperature dependencies	Q_{10} function (see Collatz *et al*., 1991)	Exponential function (see Sharkey *et al*., 2007)	Exponential function (see Sharkey *et al*., 2007)
Rubisco kinetic constants	Q_{10} temp. Coefficients (see Collatz *et al*., 1991)	Values determined *in vivo* at c_c (see Sharkey *et al*., 2007)	Values determined *in vivo* at c_c (see Sharkey *et al*., 2007)

Table 1. Differences between the three model configurations: V_{max} (µmol CO_2 m^{-2} s^{-1}), maximum carboxylation rate of Rubisco; $\alpha_{int/app}$ (mol CO_2 mol^{-1} PAR; mol e^- mol^{-1} photons respectively), intrinsic/apparent quantum efficiency; g_i (µmol CO_2 m^{-2} s^{-1} Pa^{-1}), the internal conductance to CO_2; J_{max} (µmol e^- m^{-2} s^{-1}), maximum rate of electron transport; F_0, c_i/c_a ratio for specific humidity deficit in canopy; D_c (kg kg^{-1}), the critical humidity deficit.

	Exponential function					Q_{10} function	
	Value at 25 °C	c	ΔH_a	ΔH_d	ΔS	Value at 25 °C	Q_{10}
Parameters used for fitting							
K_o (Pa)	16582	12.3772	23.72			30000	1.20
K_c (Pa)	27.238	35.9774	80.99			30	2.10
Γ^* (Pa)	3.743	11.187	24.46			2.6	0.57
Used for normalising							
R_d (µmol CO_2 m^{-2} s^{-1})		18.7145	46.39				2.00
V_{max} (µmol CO_2 m^{-2} s^{-1})		26.355	65.33				2.00
J_{max} (µmol e^- m^{-2} s^{-1})		17.71	43.9				*n/a*
g_i (µmol CO_2 m^{-2} s^{-1} Pa^{-1})		20.01	49.6	437.4	1.4		*n/a*

Table 2. Exponential and Q_{10} temperature response functions for photosynthetic parameters and Rubisco enzyme kinetic parameters (plus values at 25 °C for model fitting). Values are taken from Bernacchi et al., (2002; 2001) and Bernacchi et al., (2003) for the exponential functions. Values are from Collatz et al., (1991) and Niinemets et al., (2009) for the Q_{10} response functions: *c,* scaling constant; ΔH_a, enthalpy of activation; ΔH_d enthalpy of deactivation; ΔS, entropy; K_o, Michaelis-Menton constant of Rubisco for O_2; K_c, Michaelis-Menton constant of Rubisco for CO_2; Γ^*, chloroplastic CO_2 photocompensation point in the absence of mitochondrial respiration; R_d, dark respiration; V_{max}, maximum carboxylation rate of Rubisco; J_{max}, maximum rate of electron transport; g_i the internal conductance to CO_2. This table is partly reproduced from Sharkey et al., (2007).

P. nigra							
Without g_i	With g_i						
♦	Δ †	†	Δ †	†	♦ Δ	♦ Δ †	♦ Δ †
V_{max}	V_{max}	J_{max}	g_i	α_{app}	α_{int}	F_0	D_c
27.92	59.11	61.12	1.12	0.11	0.076	0.875	0.07
100.73	120.69	220.23	3.01	0.18	0.076	0.875	0.07
96.91	38.41	56.25	1.27	0.24	0.076	0.875	0.07
110.00	186.54	259.96	2.70	0.19	0.076	0.875	0.07
81.93	114.39	171.27	3.70	0.14	0.076	0.875	0.07
63.71	97.62	144.62	2.07	0.09	0.076	0.875	0.07
64.26	107.24	143.76	1.73	0.14	0.076	0.875	0.07
82.43	126.00	143.66	3.74	0.22	0.076	0.875	0.07
42.70	51.04	90.61	1.85	0.11	0.076	0.875	0.07
50.41	92.80	114.01	1.17	0.15	0.076	0.875	0.07
47.88	80.50	97.47	1.27	0.14	0.076	0.875	0.07
67.34	109.41	130.07	2.73	0.20	0.076	0.875	0.07
77.07	124.77	137.99	2.13	0.20	0.076	0.875	0.07
60.59	63.45	105.74	3.70	0.20	0.076	0.875	0.07
70.48	109.75	136.23	2.07	0.20	0.076	0.875	0.07
73.05	109.75	139.58	1.73	0.21	0.076	0.875	0.07
69.84 ± 5.47	**99.47 ± 8.99**	**134.54 ± 13.04**	**2.25 ± 0.23**	**0.17 ± 0.01**	**0.076**	**0.875**	**0.07**

Table 3. Parameter values from each individual A_{net} - c_i and A_{net} - P_{PFD} response curve measured for *P. nigra*. Values in bold show the mean ± S.E. The symbols indicate which model the parameter values were used in: ♦ Model 1, Δ Model 2, † Model 3. V_{max} (µmol CO_2 m^{-2} s^{-1}), maximum carboxylation rate of Rubisco estimated with and without g_i; J_{max} (µmol e^- m^{-2} s^{-1}), maximum rate of electron transport; g_i (µmol CO_2 m^{-2} s^{-1} Pa^{-1}), the internal conductance to CO_2; $\alpha_{int/app}$ (mol CO_2 mol^{-1} quanta; mol e^- mol^{-1} quanta respectively), intrinsic/apparent quantum efficiency; F_0, c_i/c_a ratio for specific humidity deficit in canopy; D_c (kg kg^{-1}), the critical humidity deficit.

893

	Regression fit	r^2	95 % CI Intercept	95 % CI Slope	Correlation F (1, 190 *d.f*)	Correlation P	RMSD
Model Testing							
Model 1	y = -1.26 - 1.06*x*	0.98	0.38 ***	0.02 ***	9412	< 0.001	1.68
Model 2	y = 0.14 - 0.77*x*	0.93	0.69 ***	0.03 ***	2413	< 0.001	5.86
Model 3	y = -0.97 - 1.08*x*	0.98	0.37 ***	0.02 ***	9678	< 0.001	1.71
Model Calibration							
Model 1	y = -1.16 - 1.00*x*	0.76	1.41	0.08	614.3	< 0.001	5.34
Model 2	y = 1.08 – 0.72*x*	0.80	1.13 *	0.09 ***	775	< 0.001	7.18
Model 3	y = -1.44 - 1.09*x*	0.76	1.45	0.09	594.9	< 0.001	5.35
Model $_{def}$	y = 1.12 - 1.71*x*	0.71	1.43	0.16 ***	463.1	< 0.001	9.42
Model Validation							
A_{net}					$F^{\dagger}$		
Model 1	y = 1.45 - 0.84*x*	0.77	0.72 ***	0.06 ***	763.4	< 0.001	3.36
Model 3	y = 1.96 - 0.77*x*	0.72	0.78 ***	0.06 ***	589.2	< 0.001	3.91
g_s							
Model 1	y = 8.50 - 0.90*x*	0.82	13.61	0.05 ***	1083	< 0.001	65.45
Model 3	y = 1.89 - 0.93*x*	0.86	12.32	0.05 ***	1403	< 0.001	58.23

894 **Table 4.** Quantitative measures of the ability of the models to predict observed rates of A_{net} during
895 model testing and model parameterisation. The units of RMSD are (μmol CO_2 m^{-2} s^{-1}) A_{net} and
896 (mmol H_2O m^{-2} s^{-1}) for g_s. CI refers to the 95 % confidence interval surrounding the estimate of the
897 regression line intercept/slope. The stars indicate whether the intercept/slope is significantly different
898 to zero/one respectively: *** p < 0.001, ** p < 0.01, * p < 0.05. $F^{\dagger}$ indicates *P. nigra* is analysed on
899 1, 230 *d.f.* for validation.

900

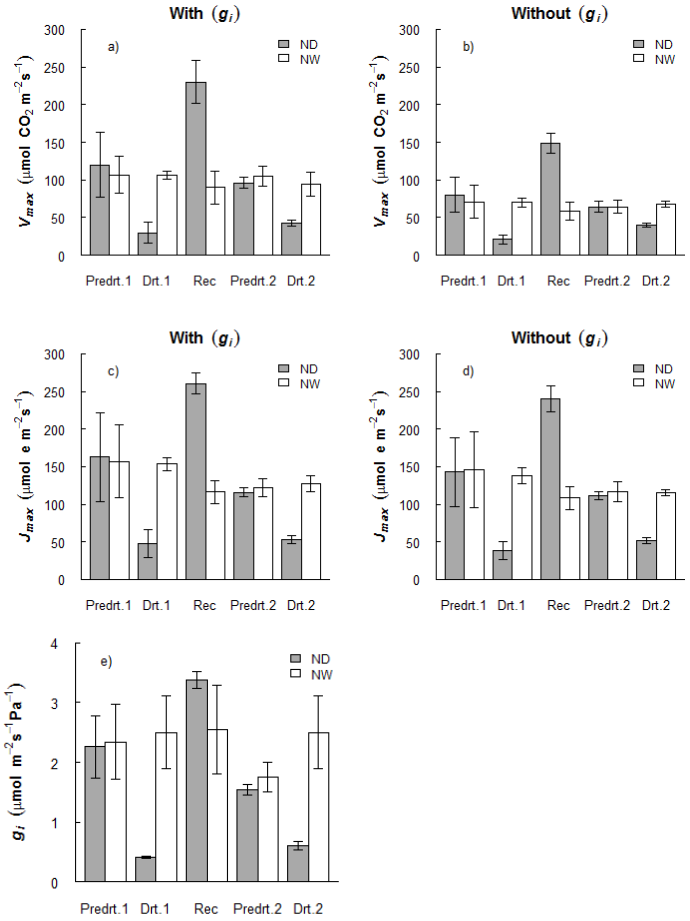

901

902 **Fig. 1.** Values of **a)** the maximum carboxylation velocity (V_{max}) estimated with internal conductance
903 to CO_2 (g_i), **b)** V_{max} estimated without g_i, **c)** the maximum rate of electron transport (J_{max}) estimated
904 with g_i, **d)** J_{max} estimated without g_i, and **e)** g_i. For each measurement period, the mean is shown ±
905 the standard error. ND and NW are stressed and control *P. nigra* trees respectively. Measurement
906 periods over the course of the experiment are denoted by; Predrt.1 = pre-drought 1 (first drought);
907 Drt.1 = first drought; Rec = recovery (re-watering of stressed trees); Predrt.2 = pre-drought 2 (second
908 drought); Drt.2 = second drought.

909

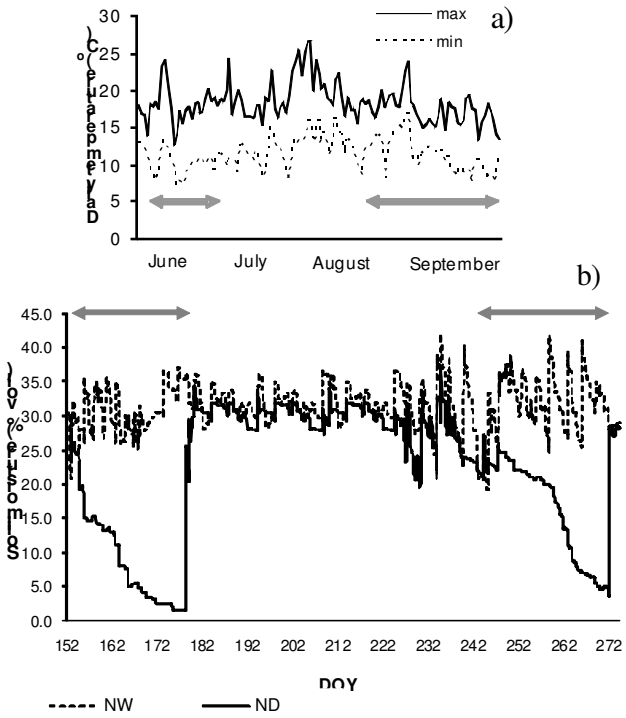

910

911 **Fig. 2.** a) Daily maximum (solid line) and minimum (dotted line) air temperatures (^{o}C), and b) hourly
912 soil moisture content (% vol.) over the experimental period (2nd June – 1st October 2008). Grey
913 arrows indicate the periods of imposed drought. NW, well-watered (control) *P. nigra* trees; ND,
914 drought treated *P. nigra* trees.
915

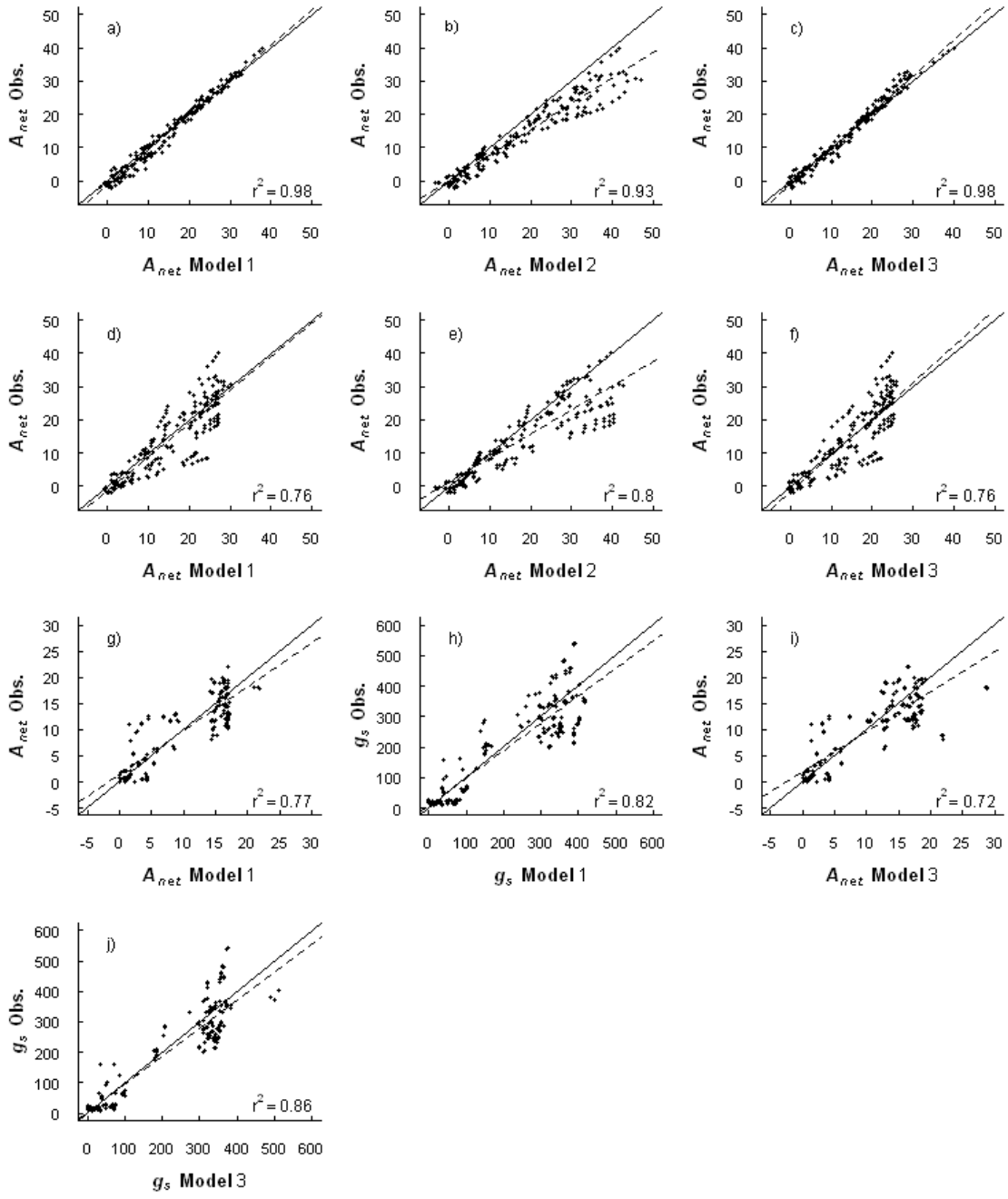

916

917 **Fig. 3.** Model testing, observed vs. predicted A_{net} (μmol m^{-2} s^{-1}) and g_s (mmol m^{-2} s^{-1}) shown for *P.*
918 *nigra*: a, b & c) model testing d, e & f) model calibration, g, h, I & j) model validation. The
919 regression line (dotted line) and r^2 are shown, along with the 1:1 line (solid line).

920